International Journal of Oceans and Oceanography
ISSN 0973-2667 Volume 1, Number 2 (2006), pp. 251-276

http://www.ripublication.com

# Neural Network-Based Estimation of Photosynthetic Efficiency

**Habtom W. Ressom[1*], Suzanne K. Fyfe[2], Siva Srirangam[3], Padma Natarajan[3], and Mohamad T. Musavi[3]**

*[1]Department of Biostatistics, Bioinformatics, and Biomathematics, Georgetown University Medical Center, 4000 Reservoir Rd, NW, Washington, DC 20057, U.S.A.*

*[2]Institute for Conservation Biology and School of Geosciences, University of Wollongong, Wollongong, New South Wales, 2522, Australia.*

*[3]Intelligent Systems Laboratory, Department of Electrical and Computer Engineering, University of Maine, Orono, ME 04469, U.S.A.*

**Abstract**

Photosynthetic efficiency is a measure of plant stress that can be used very effectively to monitor the health of vegetation, including marine plants like seagrasses. However, *in situ* measurements of the photosynthetic efficiency of seagrass meadows are time consuming, expensive, and spatially limited. In this paper, neural network-based models are developed to estimate photosynthetic efficiency from field measured spectral reflectance data for the ultimate purpose of extending such models to monitor the 'health' of vegetation through remote sensing. Variable selection and dimension reduction are applied for data preprocessing based on correlation analysis and principal component analysis, respectively. The significance of the proposed neural network-based approach is that it can model the unknown non-linear relationship between photosynthetic efficiency and spectral reflectance measurements without requiring any prior knowledge of their inherent relationship. The neural network models were compared with simple linear regression models and model trees. It was observed that the neural network model outperformed both approaches.

**Keywords:** Port Hacking, seagrass health, remote sensing, *Zostera capricorni*, *Posidonia australis*, *Halophila ovalis*, artificial neural networks, model trees.

[*] Corresponding author

## 1. INTRODUCTION

Remote sensing is an important land management tool that is widely used to provide accurate and timely synoptic information on the condition of vegetation resources of economic or environmental significance. Remote sensing has been extensively applied to assess and monitor the extent, health or productivity of agricultural crops, grazing pastures and rangelands, forestry resources, and both terrestrial and marine conservation reserves. Vegetation indices (VIs) are spectral reflectance indices calculated from remote sensing data that are commonly used to predict vegetation biomass and the leaf area index (LAI), but they have also been used to estimate yield, productivity and canopy photosynthetic capacity [1].

The recent development of new high spectral, spatial and radiometric resolution airborne and satellite-based sensors has significantly increased the potential for monitoring the 'health' of vegetation by remote sensing. Remote sensing offers a rapid, non-invasive and cost effective alternative to biochemical methods of obtaining information on plant photosynthesis, pigment content, nutrition and stress. A vast array of hyperspectral reflectance and derivative indices have been developed and tested to predict the biophysical characteristics [2, 3] and physiological status [1, 4] of agricultural crops. For example, the position of the 'red edge' derived from the maximum point of inflexion of the first derivative spectrum is strongly correlated with chlorophyll concentration, which is often considered a surrogate for plant vigour and photosynthetic capacity [5, 6]. Narrow band VIs have been applied to predict green biomass as well as chlorophyll content [3, 7-11] and more direct symptoms of stress in diseased or deficient plants including leaf chlorosis and necrosis [12-16]. This drive to produce robust and generally applicable hyperspectral VIs has not only come from their potential application in high spectral resolution remote sensing but from their current use in ground based spectroradiometry at the leaf and canopy scale.

The majority of VIs target changes in leaf pigment concentration or plant canopy geometry (e.g. LAI or biomass) that indicate a decline in the health of vegetation. However, a much earlier symptom of stress in plants is the onset of photoinhibition of photosynthesis. Photoinhibition occurs when photosynthetic rates are depressed either due to damage to the photosynthetic apparatus or by a photoprotective mechanism known as the light-dependent down-regulation of the quantum yield of photosynthesis [17-19]. During down-regulation, harmful levels of energy absorbed by light harvesting pigments are dissipated as heat by the interconversion of the xanthophyll cycle carotenoids in response to excess light energy [18, 20]. Photoinhibition is primarily a response to excess irradiance but other environmental stressors such as nutrient deficiencies, toxic pollutants, temperature extremes, and changes in salinity and pH exacerbate the onset and impact of photoinhibition [21, 22]. Hence photoinhibition will occur under normal irradiance conditions when a plant has been stressed by other environmental factors.

The chlorophyll-*a* fluorescence parameter, $F_v$:$F_m$, is a measure of the instantaneous photochemical efficiency of photosystem II (or simply photosynthetic efficiency). Decreases in $F_v$:$F_m$, have been associated with a wide range of environmental

stressors that directly affect photosystem II efficiency resulting in photoinhibition [23, 24]. Photosynthetic efficiency (PE) has previously been estimated from spectral reflectance data using the Photochemical Reflectance Index (PRI) [10, 25], which has consistently correlated with $F_v$:$F_m$ across a range of species, functional types and stress conditions in both ground level and airborne remote sensing data [26-28]. However, the PRI does not always successfully predict plant stress [16].

The results of laboratory stress experiments with the seagrass *Zostera capricorni* suggested that PE may not be satisfactorily estimated using the PRI for this group of plants [29]. Fyfe's [29] experiments showed that *Z. capricorni* plants grown at high irradiance levels suffered significant depression of PE within 1-2 weeks of treatment, corresponding with significant changes in the xanthophyll cycle carotenoids and in the visible spectral reflectance measured from their leaves. Although there was significant correlation between PE and the PRI, the relationship was very weak ($r$ = 0.361).

The awareness that healthy seagrass meadows are extremely important for the ecological functioning of coastal and estuarine ecosystems [30] has necessitated better understanding and management of this resource [31], and a requirement for regular monitoring in some parts of the world (e.g. Australia, [32]). Seagrass meadows have a significant impact on commercial resources, particularly fisheries, and therefore have high economic significance [33-36]. However, coastal waterways and their catchments have not been well managed under the pressure of agricultural, residential, commercial and industrial development. As a result, seagrass loss has been reported worldwide and in many cases, the loss has been as high as 100%. Increased anthropogenic inputs to coastal waters, in particular fine sediments, nutrients and pollutants have been predominantly linked to seagrass dieback. In addition, direct meadow damage has been caused by land reclamation, dredging, mining, training wall, wharf and marina construction, and the hydrological changes associated with these processes.

Seagrasses are marine angiosperms which respond to stress in much the same way as terrestrial higher plants [37]. The epiphytic algae that naturally grow on the surface of the seagrass leaves are typically even more sensitive to light levels, pollutants, salinity and other stress factors in an estuary than are the seagrass plants themselves [38]. Since chlorophyll *a* is a predominant light harvesting pigment in all major classes of epiphytic algae [39], the epiphytes' photoinhibitory response to stress contributes to the overall measurement of PE from a seagrass leaf or canopy. Hence, PE measured from seagrass leaves with pulse-amplitude modulated (PAM) fluorometers has been effectively used to detect declines in seagrass photosynthetic health resulting from the effects of heavy metals, petrochemicals and other toxic pollutants [40-42], excess irradiance and UV [37, 43], osmotic stress [44] and combined environmental stress factors [45]. PE is also reduced by a range of other factors that induce physiological stress in seagrass meadows including inorganic carbon limitations, nutrient deficiencies, desiccation, changes in pH and temperature. Therefore, PE is a useful early indicator of impacts on seagrass ecosystems from a wide range of human activities that influence the water quality or hydrological regime

in an estuary or bay.

Remote sensing and more often, aerial photography, have been widely used to map the distribution of seagrass meadows, but monitoring changes in meadow extent does not provide information about meadow condition until after large scale dieback events have already occurred [46]. The monitoring of biophysical variables such as standing crop, biomass, shoot density or LAI using field surveys or remote sensing [47, 48] may provide a more accurate measure of meadow deterioration but again, only after significant and possibly irreversible dieback has already occurred. An early warning of potential seagrass dieback can be achieved by directly monitoring physiological variables associated with plant stress, such as PE. The use of divers to measure PE *in situ* with submersible PAMs (diving-PAMs) [49] is time consuming, expensive and spatially limited. The advantage of remote sensing over field based methods for monitoring the condition of seagrasses is that it is possible to acquire a synoptic overview of a large meadow or whole estuary in a fraction of the time and effort it would take to measure the same area by boat. In addition, broad scale patterns and trends in photosynthesis or stress can only be identified using spatially relevant data. Indeed, management agencies and the scientific community generally agree that monitoring should be undertaken at an ecosystem level.

Reflectance indices are linear combinations of usually 2-3 pre-selected wavelengths that are related to vegetation parameters using simple linear regression or correlation. However, the relationship between spectral reflectance and PE is often complex, non-linear and of second order. Artificial neural networks can play a vital role in monitoring seagrass meadows in a complex oceanic environment over wide spatial and temporal scales. The advantage of using neural networks is that they are flexible towards the choice of inputs. They are tolerant towards noise and have the ability to learn from data without requiring any prior knowledge of the relationship between the input and output variables used. Moreover, they can deal with non-linear relationships effectively [50].

The spectral reflectance data obtained using imaging spectrometers and spectroradiometers are generally high dimensional and therefore input dimension reduction or input variable selection is a critical issue in the analysis of such data. Popular methods for dimension reduction have been principal component analysis and correlation analysis. Correlation analysis enables the selection of the input variables based on their correlation with the output variable. It also helps in removing redundant inputs. Principal component analysis (PCA) performs a linear projection from the original high dimensional input space to a lower dimensional new space such that the derived variables (principal components) in the new space are uncorrelated and contain the main portion of information in the original input space.

In this paper, four experiments were conducted to build neural network based models that estimate PE from field measured spectral reflectance data. The performance of the models was compared with simple linear regression model and model trees. Data standardization, correlation analysis and PCA were used for data preprocessing. The different experiments and approaches were analyzed with regard to their applicability

on remote sensing data. The goal of the experiments was to develop a reliable neural network based model on the field data, which can be extended to monitor seagrass ecosystem 'health' through remote sensing.

## 2. BACKGROUND

### *2.1 Simple linear regression model*

Linear regression models are the most commonly used methods for finding the best linear fit that relates the target values of the training cases to the values of their inputs. The quality of the model thus created is judged by its ability to estimate the target values of previously unseen input values. Hence, once the optimal parameters of a linear regression model are determined using the linear least squares method, the performance of the resulting model is tested upon previously unseen samples.

### 2.2 Model trees

In building model trees (MTs), the input space is split into subspaces and a separate linear model (LM) is created for each subspace. The idea of splitting the data into subspaces is similar to decision tree, but instead of the class labels, MTs have linear regression functions at their leaves [51, 52]. Therefore, they are analogous to piece-wise linear functions and hence they can be used to model nonlinear relationships. The M5 algorithm is used for inducing a model tree [53]. As shown in Figure 1, the algorithm splits the training samples into N subsets. The splitting criterion for the M5 model tree algorithm is based on treating the standard deviation of the class values that reach a node as a measure of the error at that node, and calculating the expected reduction in this error as a result of testing each attribute at that node. After examining all possible splits, M5 chooses the one that maximizes the expected error reduction. Splitting in M5 ceases when the class values of all the instances that reach a node vary just slightly, or only a few instances remain. Detailed description of M5 algorithm can be found in [53].

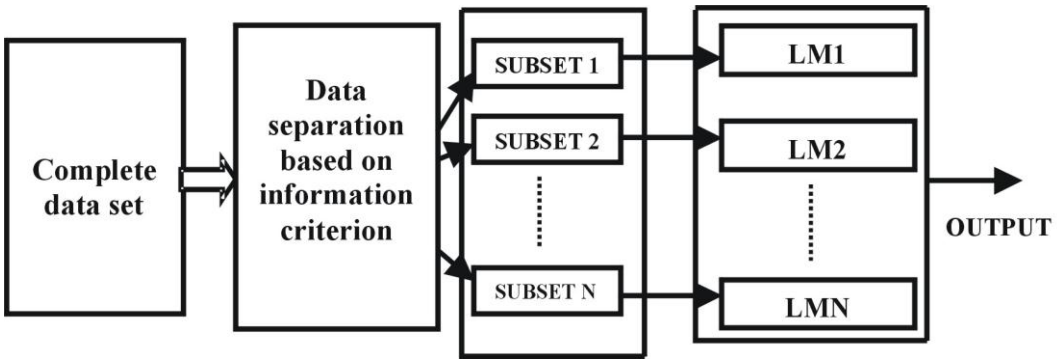


**Figure 1.** General representation of the M5 algorithm to create model trees.

2.3 Artificial Neural Networks

An artificial neural network (ANN) consists of many simple computational elements arranged in layers and operating in parallel. The way the neurons are connected defines the architecture of the network. A class of ANNs, where the input feeds forward through the network layers to the output, is referred to as a feedforward network (e.g. a multilayer perceptron, MLP). This kind of network is known to be capable of learning complex input-output mapping, i.e., given a set of inputs and desired outputs or targets, an adequately chosen neural network can emulate the mechanism that produces the data through learning. The weights, which define the strength of connection between the nodes, are adapted during typical training to yield good performance.

Once suitable network architecture (e.g. number of neurons and number of hidden layers for an MLP) has been selected, a number of parameters are set for the training. These include the learning method and strategy (e.g., back-propagation, Gauss-Newton, and Levenberg-Marquardt), stopping conditions, and learning rate. During the training phase, the training data from the input files are presented to the network and the connection weights between the neurons are determined. Training is completed when the specified stopping conditions are fulfilled. To avoid over training the performance of the network on validation data set is used as a stopping criterion. After the training is completed, the network's generalization capability is tested using previously unseen data (i.e., test dataset).

## 3. MATERIALS AND METHODS

### 3.1 Study Site

The data used in this study were obtained from Port Hacking, New South Wales, Australia, a drowned river valley estuary located about 24 km south of (central) Sydney at 151°10'E 34°05'S (Figure 2). Port Hacking is bounded on the northern side by the southern suburbs of Sydney and on the southern side by the Royal National Park. The Hacking River and several small creeks whose catchments occur predominantly within the national park feed the estuary, however, freshwater inputs are relatively small and the hydrodynamics of the estuary are dominated by tidal flows. The estuary has extremely good water quality because of strong tidal flushing (mean spring tidal range is approximately 1.32 m), very little industrial and no agricultural inputs, although the effects of storm water discharge and suburban runoff can be observed in the northern bays.

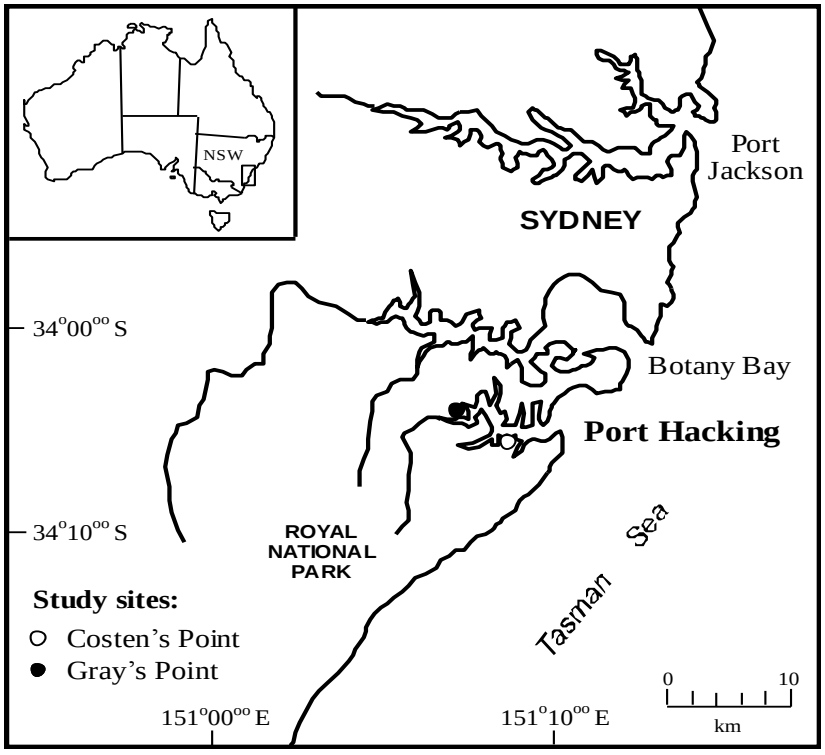


**Figure 2:** Location of the study sites where the data were collected.

### 3.2 Data Used

The data used in this study consisted of field-based spectral reflectance measurements in the range 430-900 nm and associated PE measurements of three different seagrass species: *Zostera capricorni*, *Posidonia australis* and *Halophila ovalis*. A total of 86 samples were considered in this study. The seagrass leaf samples of all three species (*n*=20 *Z. capricorni*, n=22 *P. australis* and *n*=23 *H. ovalis* samples) were cut haphazardly from Costen's Point, Port Hacking within a meadow area of approximately 0.25 ha in water depths ranging from 0.5-3 m. The detached leaves were placed into black plastic bags filled with seawater without removing the leaves or bags from the water column. Leaf samples of *Z. capricorni* (*n*=21 samples) were similarly cut from depths of around 1-2 m in a monospecific meadow at Gray's Point, Port Hacking and placed in a black plastic bag. The bags were hung in the estuary to dark-adapt the leaves for 20 minutes prior to measurement while maintaining leaf temperatures at the estuary water temperature. The PE of each of the leaf samples was measured as $F_v$: $F_m$ using a Pulse-Amplitude Modulated flourometer (PAM 2000, Walz, Effeltrich, Germany) inside the dark environment of the bags after bringing the bags on board the boat and draining them of water. Each leaf sample was removed from the bag immediately after PE measurement and placed on a black, non-reflective background in full sunlight so that the spectral reflectance of each leaf sample could be measured using an ASD Fieldspec-FR spectroradiometer according to the methods described in [54]. Measurements were taken from handful-sized clumps of intact

leaves, complete with the surface layer of fouling organisms which occurs naturally on seagrass leaves and is dominated by small macroalgal epiphytes. Canopy leaves in temperate Australian seagrass meadows are rarely observed without a moderate to heavy growth of epibionts. Since the canopy dominates the signal received by a remote sensing instrument, it is important to measure the responses of mature, fouled leaf samples from the top 10-15cm of the canopy in order to develop models applicable to the remote sensing of seagrass meadows.

### 3.3 Data Pre-Processing and Model Development

To get insight into the relationship between spectral reflectance and PE, we compared the spectral reflectance of the *Z. capricorni* from Costen's Point and Gray's Point showing relatively low PE (< 0.62) with those displaying high PE (> 0.72) (Figure 3). These two PE ranges represent stressed (photoinhibited) seagrasses and relatively healthy seagrasses, respectively. Overall, the stressed seagrass samples have lower reflectance in the NIR than the health samples. This is a characteristic stress response for plants that is associated with internal structural changes in the leaves and cell contents [55, 56]. However, we see that individual PE measurements display a complex relationship with their corresponding spectral reflectance at various wavelengths. To get more insight into this relationship, we conducted correlation analysis. Figure 4 shows a plot of correlation coefficient (R) that resulted when PE is correlated with spectral measurement at each individual wavelength in the reflectance spectrum (430-900 nm). As shown in the figure, the peak regions of correlation between spectral reflectance and PE occurred between 430-434 nm, 546-565 nm and 696-712 nm.

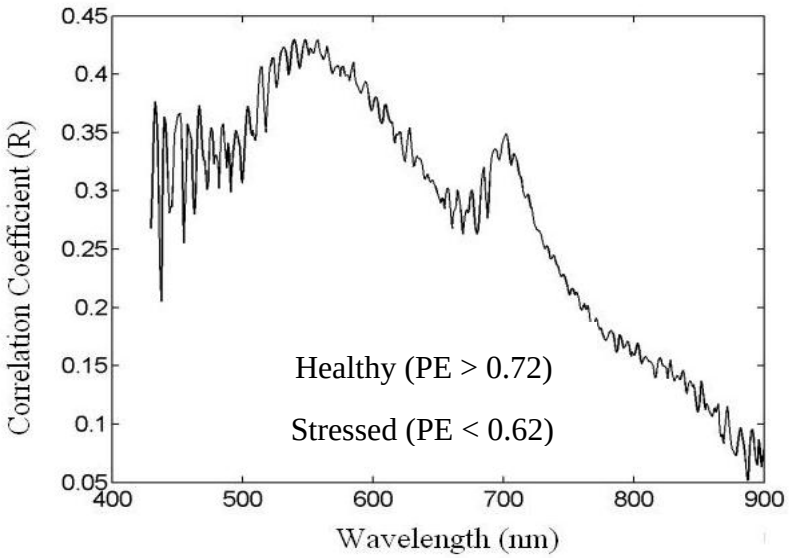


**Figure 4:** Plot of correlation coefficient (R) obtained when PE is correlated with spectral reflectance measurement at each individual wavelength in the reflectance spectrum (430-900 nm).

We developed multi-layer feed-forward neural network models to estimate PE from spectral reflectance measurements. The input variables (spectral reflectance measurements) and the output (PE) were standardized to have zero mean and unit standard deviation prior to model development. Correlation analysis and principal component analysis were used for variable selection and dimensionality reduction.

The Levenberg-Marquardt learning algorithm was used to train the neural network models. 50% of the data samples were used for training, 25% for validation and the remaining 25% for testing. The performance of the network on validation data set was used as a stopping criterion to prevent overfitting. The generalization capability of the network was tested using previously unseen testing data. Optimal network structure was obtained after experimenting with different number of hidden layers and neurons. The performance of the neural network models was compared with simple linear regression models as well as model trees.

## 4. EXPERIMENTAL TESTS

Four experiments were carried out each with a different set of variables. Variable selection and data preprocessing were done using correlation analysis, principal component analysis, and by extracting relevant features such as integrals, peak-to-peak, and averages over a given spectral band. In each experiment, three models were developed using simple linear regression model, model trees, and neural networks. Weka software [52] was used to apply M5 algorithm for model trees.

### 4.1 Experiment 1

Based on correlation analysis, five spectral reflectance measurements corresponding to the peak regions (435 nm, 553 nm, 562 nm, 700 nm and 710 nm) were chosen as model inputs. The model target was PE. The simple linear regression model obtained for this experiment is given below.

$$PE = 0.646 + 0.00626R_{435} + 1.28R_{553} - 2.79R_{562} + 1.21R_{700} - 0.227R_{710}$$

where PE is the model target $R_{435}$, $R_{553}$, $R_{562}$, $R_{700}$ and $R_{710}$ are the reflectance measurements at 435 nm, 553 nm, 562 nm, 700 nm and 710 nm, respectively.

The model tree obtained for the experiment is shown below.

$R_{553} \leq 0.0519$: LM1
$R_{553} > 0.0519$:
| $R_{435} \leq 0.062$: LM2
| $R_{435} > 0.062$:
    | $R_{553} \leq 0.126$: LM3
    | $R_{553} > 0.126$: LM4

where the models at the leaves in the above tree are represented by the following equations:

LM1: $PE = 0.734 - 1.64R_{553} - 0.257R_{562}$

LM2: $PE = 0.608 - 0.913R_{435} + 4.86R_{553} - 4.41R_{562} - 0.253\,R_{700} + 0.0561\,R_{710}$

LM3: $PE = 0.497 + 1.190R_{435} + 9.74R_{553} - 9.54R_{562} - 0.198\ R_{700} + 0.0341\ R_{710}$

LM4: $PE = 0.592 + 0.333R_{435} + 5.96R_{553} - 6.11R_{562} - 0.200\ R_{700} + 0.0341\ R_{710}$

For the neural network model, after experimenting with different number of hidden layers and neurons, an optimal 5-9-3-1 structure, with five inputs and two hidden layers with nine and three nodes in each layer and one output node, was reached. In this experiment as well as the experiments in the following sections, it was observed that neural networks and model trees performed much better than the linear regression models. As a result, we present scatter plots for these former two models only. Figure 5 shows the scatter plot between measured and estimated PE obtained by the neural network model and the model tree for the entire dataset (training, validation, and test).

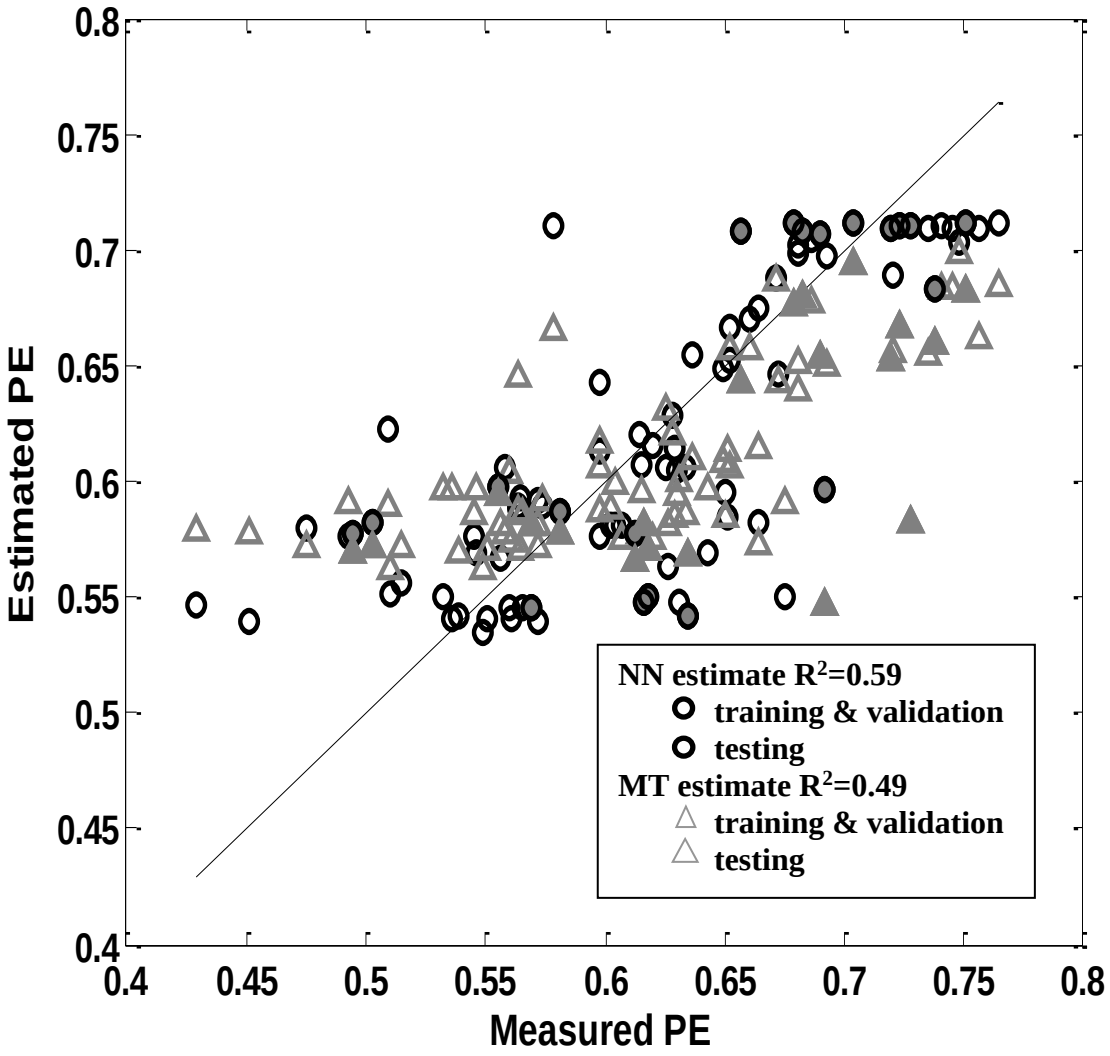


**Figure 5:** Measured and estimated PE for Experiment 1.

### 4.2 Experiment 2

In this experiment, the entire input space (430-900 nm) was initially integrated. A total of eleven inputs were used in the model. These include the five spectral reflectance measurements used in Experiment 1 (435 nm, 553 nm, 562 nm, 700 nm and 710 nm) and six additional features. The features include the peak-to-peak value over the entire band and integrals of the reflectance measurements between 430 and 435 nm, 430 and 553 nm, 430 and 562 nm, 430 and 700 nm, 430 and 710 nm. The simple linear regression model obtained for the experiment is described by the equation below.

$$PE = 0.625 + 0.0285R_{435} - 0.199R_{553} + 0.191R_{562} + 0.0503R_{700} - 0.0391R_{710} - 1.01\sum_{430}^{435}R - 3.02\sum_{430}^{553}R + 1.29\sum_{430}^{562}R + 0.129\sum_{430}^{700}R - 1.32\sum_{430}^{710}R + 0.674R_{p2p}$$

where $\sum_{\alpha}^{\beta}R$ denotes the sum of the reflectance measurements for the wavelengths between $\alpha$ and $\beta$ nm; $R_{p2p}$ represents the peak-to-peak reflectance measurement over the entire spectra.

The model tree method obtained for the experiment is shown below.

$R_{435} \leq 0.139$: LM1

$R_{435} > 0.139$: LM2

where the models at the leaves are represented by the following equations:

LM1: $PE = 0.665 + 0.543\sum_{430}^{700}R - 0.834\sum_{430}^{710}R + 0.305R_{p2p}$

LM2: $PE = 0.597 + 0.247\sum_{430}^{700}R - 0.379\sum_{430}^{710}R + 0.139R_{p2p}$

For the neural network model, after experimenting with different number of hidden layers and neurons, an optimal 11-17-7-1 structure was reached. Figure 6 shows scatter plots for the neural network model and the model tree for the entire dataset.

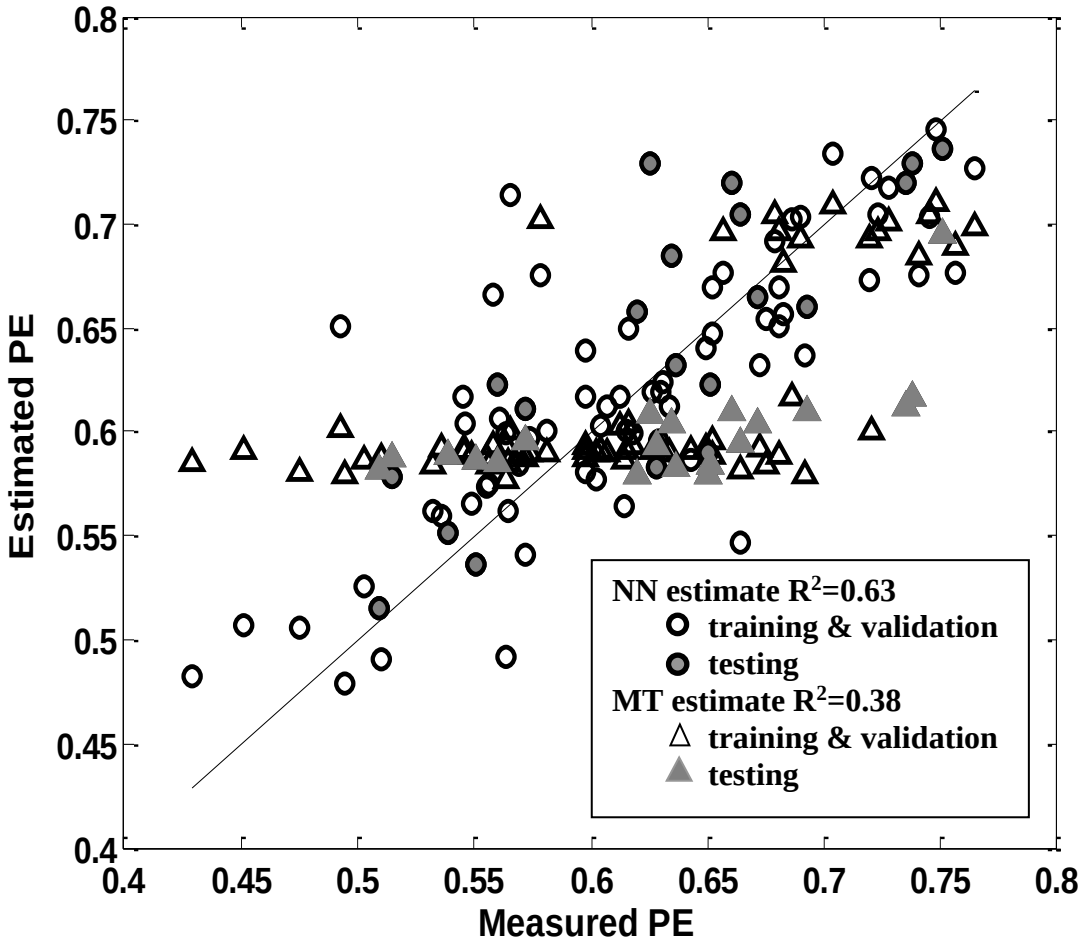


**Figure 6:** Measured and estimated PE for Experiment 2.

### 4.3 Experiment 3

In this experiment, inputs to the model include spectral reflectance measurements from the peak regions of the correlation plot in Figure 4. These include spectral reflectance measurements from regions 430-434 nm, 546-565 nm and 696-712 nm. A total of 43 spectral measurements were used as inputs to the model. The input and output variables were standardized to have zero mean and unit standard deviation. PCA was applied to reduce the dimension of the input space, where 3 principal components (out of 43) explained more than 99.5 % of the variance in the data. Thus, the three principal components were used as inputs to the model.

The simple linear regression model obtained for the experiment is described by the equation below.

$$PE = 0.625 + 0.00362PC_1 + 0.00374PC_2 - 0.0305PC_3$$

where $PC_1$, $PC_2$ and $PC_3$ are the first, second and third principal components which when combined together contribute more than 95% of the variance of the dataset.

The model tree obtained for the experiment is as follows:

$PC_1 \leq 5.02$ :

| $PC_3 \leq -0.293$ : LM1

| $PC_3 > -0.293$ : LM2

$PC_1 > 5.02$ : LM3

The corresponding models at the leaves are:

LM1: $PE = 0.623 + 0.000823PC_1 - 0.0072PC_3$

LM2: $PE = 0.6 + 0.000823PC_1 - 0.0072PC_3$

LM3: $PE = 0.651 + 0.00173PC_1 - 0.0679PC_3$

For the neural network model, after experimenting with several network structures, an optimal 3-6-3-1 architecture was reached. Figure 7 shows the scatter plots for the neural network model and model tree for the entire dataset.

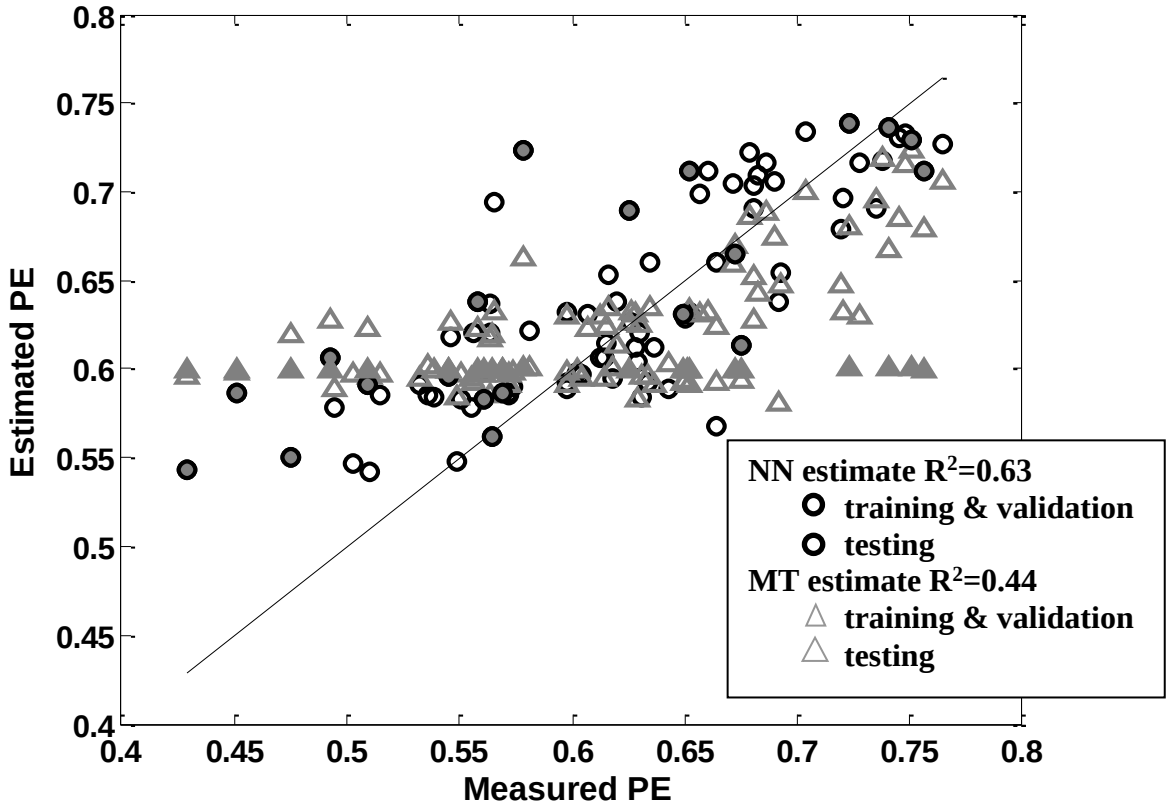


**Figure 7:** Measured and estimated PE for Experiment 3.

**4.4 Experiment 4**

In this experiment, three bands, each 10 nm wide i.e., 431-440 nm, 556-565 nm and 695-704 nm from the peak regions of the correlation plot, were selected and each of the three bands were averaged. The resulting three averaged bands were used as inputs to the model. The simple linear regression model obtained for the experiment is described by the equation below.

$$PE = 0.669 + 0.496\overline{R}_{431\text{–}440} - 1.56\overline{R}_{556\text{–}565} + 0.461\overline{R}_{695\text{–}704}$$

where $\overline{R}_{\alpha-\beta}$ denotes the band average reflectance between $\alpha$ and $\beta$ nm.

The model tree obtained for the experiment is given below.

$\overline{R}_{556\text{–}565} \leq 0.0497$: LM1

$\overline{R}_{556\text{–}565} > 0.0497$:

| $\overline{R}_{556\text{–}565} \leq 0.13$: LM2

| $\overline{R}_{556\text{–}565} > 0.13$: LM3

where the models at the leaves are given by:

$$LM1: PE = 0.691$$

$$LM2: PE = 0.507 + 0.767\overline{R}_{695\text{–}794}$$

$$LM3: PE = 0.562$$

For the neural network model the input and output variables were standardized to have zero mean and unit standard deviation before presenting it to the neural network. After experimenting with several network structures, an optimal 3-5-2-1 architecture was reached. Figure 8 depicts the scatter plots for the neural network and the model tree for the entire dataset.

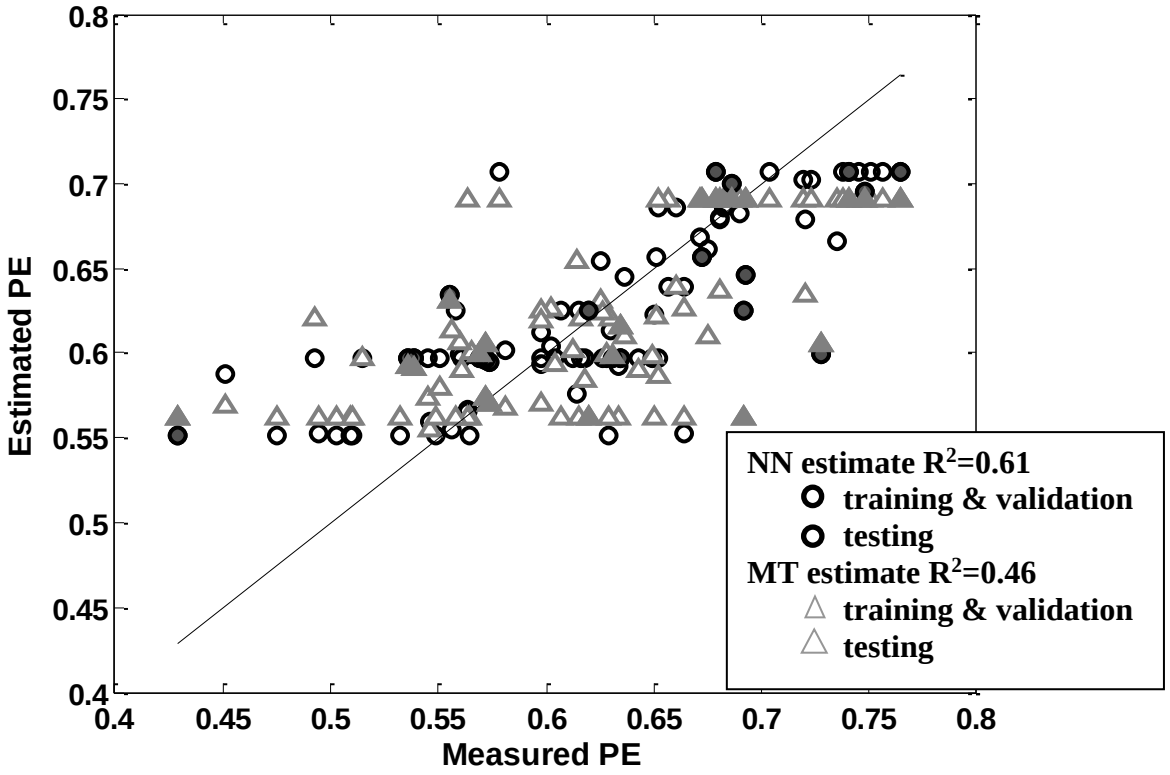


**Figure 8:** Measured and estimated PE for Experiment 4.

## 5. DISCUSSION AND CONCLUSIONS

Table 1 summarizes the performances of the three types of models (simple linear regression models, model trees, and neural networks) created in this paper for four experiments. As shown in the table, neural network models outperformed both the simple linear regression model and the model trees in all experiments in terms of coefficient of determination ($R^2$) and root mean squared error (RMSE).

**Table 1:** Summary of the Models Developed to Estimate PE in Seagrasses from Spectral Reflectance Data.

| | **Exp 1** | **Exp 2** | **Exp 3** | **Exp 4** |
|---|---|---|---|---|
| **Variable and feature selection** | correlation analysis | correlation analysis, integrals, and peak-to-peak | correlation analysis and PCA | correlation analysis, three 10nm band averages |
| **Total # of actual inputs** | 5 | 471 | 43 | 30 |
| **# of inputs selected** | 5 | 11 | 3 | 3 |
| $R^2$ for training data | | | | |
| **Simple linear regression model** | 0.18 | 0.41 | 0.15 | 0.27 |
| **Model tree** | 0.53 | 0.43 | 0.51 | 0.46 |
| **NN model** | 0.59 | 0.62 | 0.64 | 0.61 |
| $R^2$ for test data | | | | |
| **Simple linear regression model** | 0.31 | 0.54 | 0.40 | 0.17 |
| **Model tree** | 0.42 | 0.40 | 0.46 | 0.46 |
| **NN model** | 0.57 | 0.66 | 0.67 | 0.61 |
| RMSE for training data | | | | |
| **Simple linear regression model** | 0.067 | 0.059 | 0.061 | 0.062 |
| **Model tree** | 0.053 | 0.059 | 0.048 | 0.053 |
| **NN model** | 0.048 | 0.048 | 0.041 | 0.045 |
| RMSE for test data | | | | |
| **Simple linear regression model** | 0.064 | 0.047 | 0.093 | 0.081 |
| **Model tree** | 0.065 | 0.065 | 0.085 | 0.063 |
| **NN model** | 0.052 | 0.044 | 0.072 | 0.057 |

Table 1 and Figures 5-8 show that Experiments 2 and 3 gave overall better performance than the other two experiments. Note that in Experiment 2, the models needed the entire 430-900 nm space for integrals to be performed. The advantage of the other three experiments over Experiment 2 is the fact that they require reflectance measurements collected from a lower number of wavelengths in order to predict photosynthetic efficiency. Experiment 3 compresses reflectance measurements at 43 wavelengths into three using PCA. In Experiment 1, reflectance measurements at only five wavelengths are required. Thus, it is more applicable in circumstances where memory or processing time is a limitation. In addition, monitoring can be simplified and made more cost effective using purpose built or programmed instruments that measure only the 5 wavebands of interest. For example, PRI has been measured in the field from agricultural crops using a portable 'leaf reflectometer' developed for this purpose [57, 58].

The peak regions of correlation between spectral reflectance and PE (Figure 4) occurred between 430-434 nm, 546-565 nm and 696-712 nm since these regions correspond to the regions of maximum chlorophyll *a* and carotenoid absorption in the blue wavelengths, minimum absorption by photosynthetic pigments (i.e., maximum visible reflectance) in the green wavelengths and at the red edge, respectively.

The red edge is the rapid rise seen in the spectral reflectance curve of green plants at the boundary between maximum chlorophyll *a* absorption of red wavelengths and the lack of absorption of NIR light by photosynthetic pigments. Chlorophyll *a* is responsible for the absorption of 70-90% of radiation entering a leaf [59] and this pigment clearly dominates the spectral response of both healthy and stressed plants, including many algae. However, slight differences in leaf biochemistry, internal anatomy and molecular structure induce subtle shifts in the degree and position of maximal absorption by plant pigments [55]. Seagrasses placed under sustained photosynthetic stress have responded with the photoprotective pigment changes typical of most higher plants [37, 43, 60]. In particular, stressed *Z. capricorni* leaves show increases in the proportion of the VAZ pool of xanthophyll carotenoids (violaxanthin + antheraxanthin + zeaxanthin) relative to chlorophyll content and in the proportion of the xanthophylls remaining in the de-epoxidized state following dark adaptation [29]. The spectral response recorded from stressed seagrass leaves with their layer of epiphytes in the field (Figure 3) displayed many of the reflectance changes characteristically induced by these biochemical changes. The blue shift in the green edge and increased far green – near red reflectance observed for stressed seagrass leaves are symptomatic of the de-epoxidation of the xanthophyll carotenoids into the photoprotective state [25, 61]. Longer term stress will often result in increased carotenoid:chlorophyll which induces a blue shift in the red edge as the chlorophyll begins to break down [5, 6]. This biochemical change was not apparent in the spectra of the stressed seagrasses, even though some decrease in the amount of light absorbed by chlorophyll could be observed. This finding is consistent with the spectral changes that might be expected for a short-term decrease in photosynthetic efficiency without the chlorosis that would likely occur if stress persisted over the longer term. In addition, the magnitude of NIR reflectance was clearly affected by

short term stress and it appears that stress-related changes in the spectral reflectance of fouled seagrass leaves (particularly in the green wavelengths) are influenced not only by changes in pigment concentrations but by other factors that are predominantly presumed to be related to changes in internal leaf structure and reorganization of the cell contents. These complex reflectance changes across the visible and NIR spectrum that indicate a decline in PE will not be adequately represented by a linear hyperspectral index combining only a very few, specific wavelengths that target particular pigment changes. In fact, the best regression result obtained by applying the PRI [$(R_{531}–R_{570})/(R_{531}+R_{570})$] to predict PE from the same dataset gave a coefficient of determination of $R^2 = 0.139$ (Figure 9). Neural network models that used ba ss.

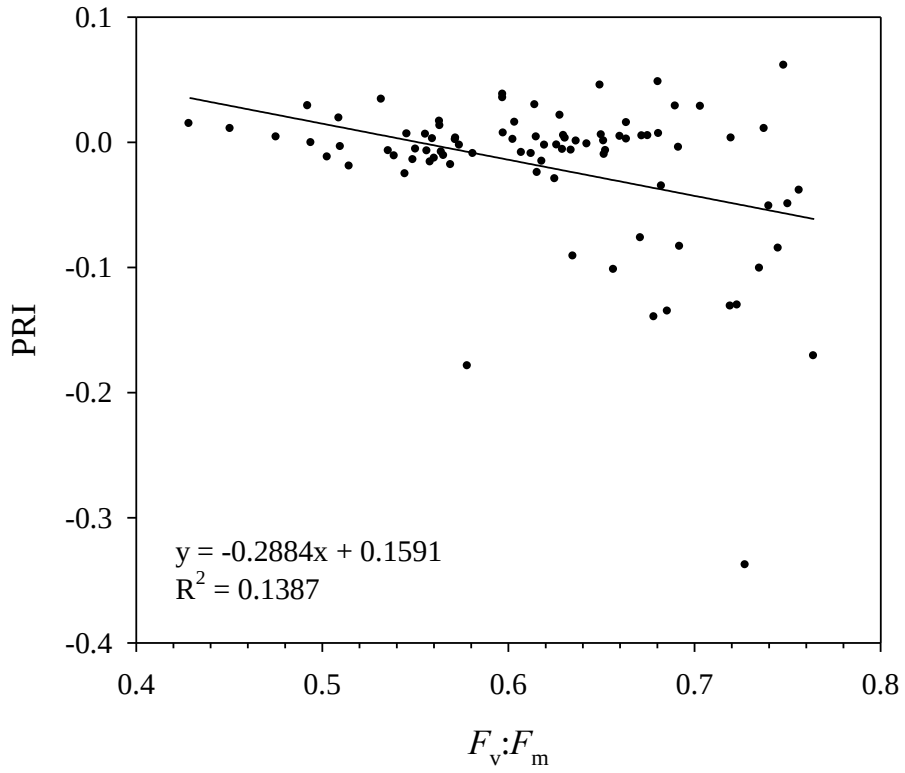


**Figure 9:** Simple linear regression of PE ($F_v$: $F_m$) with the PRI. (n = 86 leaf samples from the three seagrass species).

The applicability of models developed using field spectroradiometer data on remote sensing data depends on how accurate the models are and on the spectral and radiometric resolution of available remote sensing instruments [62]. The inputs required for the models developed in Experiments 1, 2 and 3 require truly hyperspectral instruments, i.e., with narrow, continuous bands comparable in spectral resolution and sampling interval to that of field spectrometers [63]. The 1 nm bandwidth is too narrow and specific for the half-band-widths of most sensors and such instruments are still under development. Programmable imaging spectrometers

that offer high signal-to-noise ratio such as the CASI (Compact Airborne Spectrographic Imager, Itres Inc.) or other high spectral resolution scanners with suitably placed band centers of appropriate bandwidths will be able to supply the averaged spectral data suitable for input into the model developed in Experiment 4. Since the attenuating effects of the atmosphere and a water column on the signal must also taken into account [39], the use of bands of averaged data and therefore the model developed in Experiment 4, are most applicable to operational airborne remote sensing at this stage. Traditional broadband sensors (e.g. Spot, Landsat TM) do not have the capacity to supply data applicable to NN models.

A decline in the PE measured from a seagrass meadow will rapidly indicate when the plants are suffering from photosynthetic stress. Since photoinhibition through the down-regulation of photosynthesis acts to protect the plants from damage, the change in PE will occur weeks or months before continued stress leads to dieback. The PE of seagrass meadows will be decreased by a wide range of human-induced and natural disturbances that stress the plants. These include the influx of toxic pollutants, toxic levels of nutrients and other industrial and urban discharges that change the pH, temperature or salinity of the water [40-42, 44, 64]. Photosynthetic stress will also result when hydrodynamic changes in the waterbody leave the seagrasses exposed to high light and dehydration, or restrict water movement (e.g. tidal flows) around the leaves and therefore limit the uptake of inorganic carbon and nutrients [65-67].

Seagrass dieback resulting from eutrophication or sedimentation of the waterway will not be predicted by monitoring PE unless these disturbances are accompanied by toxic effects or other stressors that affect the PE. Eutrophication is the product of high nutrient loads entering the marine environment, which stimulates excessive growth of phytoplankton and the epiphytic macroalgae attached to the seagrass leaves. Both eutrophication and sedimentation limit the amount of light penetrating to the seagrass canopy. The PE of a plant is not reduced by shading because the photosynthetic apparatus will continue to utilize whatever light energy is absorbed to fix $CO_2$ in the most *efficient* manner. Instead, the photosynthetic *rate* is reduced so less $CO_2$ is converted to carbohydrate in the process of photosynthesis. If the photosynthetic rate falls below the compensation point, the plant does not photosynthesize as rapidly as it respires, and the plant will consume its carbohydrate storage products and waste away.

The PE and spectral reflectance of the seagrasses in this study were measured from samples without removing the natural layer of fouling organisms from the surface of the seagrass leaves. Algal epiphytes are photosynthetic plants that contribute to the spectral response measured from seagrass leaves. These plants will also suffer from photosynthetic stress when environmental conditions change in the water body. Under normal conditions of growth (even in temperate estuaries where fouling of mature seagrass leaves can naturally be quite heavy) epiphytes do not mask the reflectance features of the seagrass themselves [54]. Seagrass leaves are continually turned over at a rate dependent on the species (e.g. 30-40 days for *P. australis*) so that epiphyte growth does not accumulate to a level detrimental to the plant. If epiphytic growth becomes excessive as a result of eutrophication, then it may be possible for

the epiphytes themselves to dominate the spectral response. The species composition and abundance of the epiphyte assemblage occurring on seagrass leaves can be quite sensitive to changes in water quality [38] so the spectral changes that occur in the case of eutrophication will be different to those that occur when the seagrasses suffer photosynthetic stress. Hence, there is potential for the development of neural network models to monitor this aspect of seagrass health that is complementary to the monitoring of PE since both models can be simultaneously applied to the same remote sensing data.

This research is an important step towards the operational monitoring of stress in seagrass meadows, and vegetation in general. The spectral reflectance signatures of stressed and healthy seagrass leaves differ significantly [29], but because these reflectance differences are of such small magnitude, it is yet to be determined whether remote sensing scanners will be able to detect stress in meadows through an atmosphere and water column [68]. The fact that neural network models developed in this study achieved significant accuracy and outperformed both the linear regression and model tree models suggests that there is potential for them to perform well on remote sensing data provided the images are appropriately corrected for water column and atmospheric attenuation effects. Recent advances in the application of radiative transfer theory (reviewed in [62]) has meant that spectra of benthic substrata measured by a remote sensor, including that of seagrasses (e.g. [69]), algae and corals (e.g. [70]), can increasingly be simulated accurately by radiative transfer modeling. In addition, technological progress in the spectral, spatial and radiometric resolution and signal-to-noise ratio of remote sensing instruments (hyperspectral sensors in particular) continues to increase our capacity to detect narrow spectral features associated with pigmentation and photosynthesis in submerged plants (e.g. [71]). The focus of the current study was to identify appropriate models for estimating PE from reflectance measurements. Our future goal will be to extend and test the models on airborne remote sensing imagery after correcting the attenuating effect of the atmosphere and the water column on the measured signal using radiative transfer modeling. Alternatively, new models can be built to capture the relationship between the raw remotely sensed data and the corresponding PE.

Similar NN models may prove even more effective in the remote sensing of stress and disease in commercial crops, orchards and forests. The spectral changes observed in unhealthy terrestrial plants tend to be of greater magnitude than those we observed for seagrasses, and remote detection will not be confounded by the effects of a water column. Remote sensing may be able to provide an early warning that could help prevent further large-scale dieback events in these important seagrass ecosystems.

## Acknowledgments

The work presented in this paper was in part supported by the Maine Space Grant Consortium/NASA, Award # SG-04-17 awarded to HWR. Dr. Sharon Robinson provided assistance with field work.

**REFERENCES**

[1] Field, C. B., Gamon, J. A., and Peñuelas, J., 1995, "Remote sensing of terrestrial photosynthesis," Schulze, E.-D., and Caldwell, M.M., eds, Ecophysiology of Photosynthesis, Springer, Berlin, pp. 511-527.

[2] Malthus, T. J., Andrieu, B., Danson, F. M., Jaggard, K. W., and Steven, M. D., 1993, "Candidate high-spectral-resolution infrared indexes from crop cover," Remote Sens. Environ., 46, pp. 204-212.

[3] Thenkabail, P. S., Smith, R. B., and De Pauw, E., 2000, "Hyperspectral vegetation indices and their relationships with agricultural crop characteristics," Remote Sens. Environ., 71, pp. 158-182.

[4] Peñuelas, J. and Filella, I., 1998, "Visible and near-infrared reflectance techniques for diagnosing plant physiological status," Trends in Plant Science, 3, pp. 151-156.

[5] Boochs, F., Kupfer, G., Dockter, K., and Kuhbauch, W., 1990, "Shape of the red edge as vitality indicator for plants," Int. J. Remote Sens., 11, pp. 1741-1753.

[6] Curran, P. J., Windham, W. R., and Gholz, H. L., 1995, "Exploring the relationship between reflectance red edge and chlorophyll concentration in slash pine leaves," Tree Physiol., 15, pp. 203-206.

[7] Carter, G. A., 1994, "Ratios of leaf reflectances in narrow wavebands as indicators of plant stress," Int. J. Remote Sens., 15, pp. 697-703.

[8] Carter, G. A. and Miller, R. L., 1994, "Early detection of plant stress by digital imaging within narrow stress-sensitive wavebands," Remote Sens. Environ., 50, pp. 295-302.

[9] Demetriades-Shah, T. H., Steven, M. D., and Clark, J. A., 1990, "High resolution derivative spectra in remote sensing," Remote Sens. Environ., 33, pp. 55-64.

[10] Peñuelas, J., Filella, I., and Gamon, J. A., 1995, "Assessment of photosynthetic radiation-use efficiency with spectral reflectance," New Phytol., 131, pp. 291-296.

[11] Peñuelas, J., Gamon, J. A., Griffith, K. L., and Field, C. B., 1993, "Assessing community type, plant biomass, pigment composition, and photosynthetic efficiency of aquatic vegetation from spectral reflectance," Remote Sens. Environ., 46, pp. 110-118.

[12] Blackburn, G. A., 1998, "Quantifying chlorophylls and carotenoids from leaf to canopy scales: an evaluation of some hyperspectral approaches," Remote Sens. Environ., 66, pp. 273–285.

[13] Chappelle, E. W., Kim, M. S., and McMurtrey III, J. E., 1992, "Ratio analysis of reflectance spectra (RARS): An algorithm for the remote estimation of the concentrations of chlorophyll *a*, chlorophyll *b*, and carotenoids in soybean leaves," Remote Sens. Environ., 39, pp. 239-247.

[14] Luther, J. E. and Carroll, A. L., 1999, "Development of an index of balsam fir vigor by foliar spectral reflectance," Remote Sens. Environ., 69, pp. 241-252.

[15] Malthus, T. J. and Madeira, A. C., 1993, "High resolution spectroradiometry: Spectral reflectance of field bean leaves infected by *Botrytis fabae*," Remote Sens. Environ., 45, pp. 107-116.

[16] Stone, C., Chisholm, L. A., and McDonald, S., 2003, "Spectral reflectance characteristics of *Pinus radiata* needles affected by dothistroma needle blight," Canadian J. Botany, 81, pp. 560-569.

[17] Critchley, C., 1988, "The molecular mechanism of photoinhibition – facts and fiction," Aust. J. Plant Physiol., 15, pp. 27-41.

[18] Demmig-Adams, B., 1990, "Carotenoids and photoprotection in plants: a role for the xanthophyll zeaxanthin," Biochim. Biophys. Acta., 1020, pp. 1-24.

[19] Osmond, C. B., 1994, What is photoinhibition? Some insights from comparisons of shade and sun plants.Bios. Scientific Publishers, Oxford, UK.

[20] Demmig, B., Winter, K., Kruger, A., and Czygan, F., 1987, "Photoinhibition and zeaxanthin formation in intact leaves: a possible role of the xanthophyll cycle in the dissipation of excess light energy," Plant Physiol., 84, pp. 218-224.

[21] Adams, I., W.W., Demmig-Adams, B., Verhoeven, A. S., and Barker, D. H., 1995, "Photoinhibition during winter stress: involvement of sustained xanthophyll cycle-dependent energy dissipation," Aust. J. Plant Physiol., 22, pp. 261-276.

[22] Björkman, O. and Demmig-Adams, B., 1995, "Regulation of photosynthetic light energy capture, conversion, and dissipation in leaves of higher plants," Schulze, E.-D. and Caldwell, M.M., eds, Ecophysiology of photosynthesis, Springer, Berlin, pp. 17-47.

[23] Krause, G. H. and Weis, E., 1991, "Chlorophyll fluorescence and photosynthesis: the basics," Ann. Rev. Plant Physiol. Plant Mol. Biol., 42, pp. 313-349.

[24] Schrieber, U., Bilger, W., and Neubauer, C., "Chlorophyll fluorescence as a non-intrusive indicator for rapid assessment of in vivo photosynthesis," 1995.In: Schulze, E.-D., and Caldwell, M.M., eds, Ecophysiology of photosynthesis, Ecological studies 100, Berlin, Germany, pp. 49-70.

[25] Gamon, J. A., Peñuelas, J., and Field, C. B., 1992, "A narrow-waveband spectral index that tracks diurnal changes in photosynthetic efficiency," Remote Sens. Environ., 41, pp. 35-44.

[26] Gamon, J. A., Serrano, L., and Surfus, J. S., 1997, "The photochemical reflectance index: an optical indicator of photosynthetic radiation use efficiency across species, functional types, and nutrient levels," Oecologia, 112, pp. 492-501.

[27] Sims, D. A. and Gamon, J. A., 2002, "Relationships between leaf pigment content and spectral reflectance across a wide range of species, leaf structures and developmental stages," Remote Sens. Environ., 81, pp. 337-354.

[28] Zarco-Tejada, P. J., Miller, J. R., Mohammed, G. H., Noland, T. L., and Sampson, P. H., "Canopy optical indices from infinite reflectance and canopy reflectance models for forest condition monitoring: Applied to hyperspectral CASI data," 1999.Proceedings IEEE International Geoscience and Remote Sensing Symposium, Hamburg, Germany.

[29] Fyfe, S. K., 2004, "Hyperspectral studies of New South Wales seagrasses with particular emphasis on the detection of light stress in eelgrass *Zostera capricorni*," vol. Ph.D.: University of Wollongong, Australia, pp. 387.

[30] Wood, L. L., Ferguson, R. L., and Graham, D. B., 1993, "Monitoring spatial change in seagrass habitat with aerial photography," Photogrammetric Engineering and Remote Sensing, 59, pp. 1033-1038.

[31] Hanisak, M. D. e., 2001, "Photosynthetically Active Radiation, Water Quality, and Submerged Aquatic Vegetation in the Indian River Lagoon."

[32] Ward, T., Butler, E., and Hill, B., 1998, "Environmental Indicators for National State of the Environment Reporting: Estuaries and the Sea, Australia: State of the Environment Environmental Indicator Report," CSIRO Division of Marine Research.

[33] Bell, J. D. and Pollard, D. A., 1989, "Ecology of fish assemblages and fisheries associated with seagrass beds," Larkum, A.W.D., McComb, A.J., and Shepherd, S.A. eds, Biology of seagrasses: a treatise on the biology of seagrasses with special reference to the Australian region, Elsevier, New York, NY, pp. 565-609.

[34] Durako, M. J., Murphy, M. D., and Haddad, K. D., 1988, "Assessment of Fisheries Habitat: Northeast Florida. Fla.," Mar.Res. Publ. #45, pp. 51pp.

[35] Gilmore, R. G., 1987, "Subtropical-tropical seagrass communities of the southeastern United States: Fishes and Fish Communities," Durako, M. J., Phillips, R. C., and Lewis III, R. R., eds, Proc. of the Symposium on Subtropical-Tropical Seagrasses of the Southeastern United States. Florida Dept. of Natural Resources, Bureau of Marine Research publication 42, pp. 117-137.

[36] Livingston, R. J., 1987, "Historic trends of human impacts on seagrass meadows in Florida," Florida Department of Natural Resources, St. Petersburg, FL.

[37] Dawson, S. P. and Dennison, W. C., 1996, "Effects of ultraviolet and photosynthetically active radiation on five seagrass species," Mar. Biol., 125, pp. 629-638.

[38] May, V., Collins, A. J., and Collett, L. C., 1978, "A comparative study of epiphytic algal communities on two common genera of seagrasses in eastern Australia," Aust. J. Ecol., 3, pp. 91-104.

[39] Kirk, J. T. O., 1994, Light and photosynthesis in aquatic ecosystems, 2nd ed. ed.Cambridge University Press, Melbourne, Australia.

[40] Prange, J. A. and Dennison, W. C., 2000, "Physiological responses of five seagrass species to trace metals," Mar. Poll. Bull., 41, pp. 327-336.

[41] Ralph, P. J. and Burchett, M. D., 1998, "Photosynthetic response of *Halophila ovalis* to heavy metal stress," Environmental Pollution, 103, pp. 91-101.

[42] Ralph, P. J. and Burchett, M. D., 1998, "Impact of petrochemicals on the photosynthesis of *Halophila ovalis* using chlorophyll fluorescence," Mar. Poll. Bull., 36, pp. 429-436.

[43] Flanigan, Y. S. and Critchley, C., 1996, "Light response of D1 turnover and photosystem II efficiency in the seagrass *Zostera capricorni*," Planta, 198, pp. 319-323.

[44] Ralph, P. J., 1998, "Photosynthetic responses of *Halophila ovalis* (R.Br.) Hook. *f*. to osmotic stress," J. Exp. Mar. Biol. Ecol., 227, pp. 203-220.

[45] Ralph, P. J., 1999, "Photosynthetic response of *Halophila ovalis* (R.Br.) Hook. *f*. to combined environmental stress," Aquatic Botany, 65, pp. 83-96.

[46] NOAA, U. S., "U.S. NOAA Coastal Services Center - Guide to the seagrasses of the United States of America (including U.S. Territories in the Caribbean)," U.S. National Oceanic and Atmospheric Administration. Coastal Services Center. Submerged Aquatic Vegetation: Data Development and Applied Uses. (CD-ROM). (NOAA/CSC/20116-CD), Charleston, SC, 2001.

[47] Kirkman, H., 1996, "Baseline and monitoring methods for seagrass meadows," Journal of Environmental Management, 47, pp. 191-201.

[48] Mumby, P. J., Green, E. P., Edwards, A. J., and Clarke, C. D., 1997, "Measurement of seagrass standing crop using satellite and digital airborne remote sensing," Mar. Ecol. Prog. Ser., 159, pp. 51-60.

[49] Ralph, P. J., Gademan, R., and Dennison, W. C., 1998, "In situ seagrass photosynthesis measured using a submersible pulse-amplitude modulated fluorometer," Mar. Biol., 132, pp. 367-373.

[50] Haykin, S., 1999, Neural Networks: A Comprehensive Foundation Englewood Cliffs, NJ: Prentice-Hall.

[51] Quinlan, J. R., "Learning with continuous classes," 1992.In: Proc. AI'92 (Fifth Australian Joint Conf. on Artificial Intelligence) (ed. by Adams , A., and Sterling, L.),World Scientific, Singapore, pp. 343-348.

[52] Witten, I. H. and Frank, E., 2000, Data Mining: Practical Machine Learning Tools and Techniques with Java Implementations.Morgan Kaufmann Publishers, San Francisco, USA.

[53] Solomatine, D. P. and Dulal, K. N., 2003, "Model trees as an alternative to neural networks in rainfall-runoff modeling," Hydrological Sciences Journal, 48,

pp. 399- 411.

[54] Fyfe, S. K., 2003, "Spatial and temporal variation in spectral reflectance: Are seagrass species spectrally distinct?," Limnology and Oceanography, 48, pp. 464-479.

[55] Gates, D. M., Keegan, H. J., Schleter, J. C., and Weidner, V. R., 1965, "Spectral properties of plants," Appl. Optics, 4, pp. 11-20.

[56] Vogelmann, T. C., 1989, "Yearly Review: Penetration of light into plants," Photochem. Photobiol., 50, pp. 895-902.

[57] Gamon, J. A. and Surfus, J. S., 1999, "Assessing leaf pigment content and activity with a reflectometer," New Phytol., 143, pp. 105-117.

[58] Méthy, M., 2000, "A two-channel hyperspectral radiometer for the assessment of photosynthetic radiation-use efficiency," J. Agric. Engng Res., 75, pp. 107-110.

[59] Curran, P. J., 1989, "Remote sensing of foliar chemistry," Remote Sens. Environ., 30, pp. 271-278.

[60] Ralph, P. J., Polk, S. M., Moore, K. A., Orth, R. J., and Smith Jr., W. O., 2002, "Operation of the xanthophyll cycle in the seagrass *Zostera marina* in response to variable irradiance," J. Exp. Mar. Biol. Ecol., 271, pp. 189– 207.

[61] Gamon, J. A., Field, C. B., Bilger, W., Björkman, O., Fredeen, A. L., and Peñuelas, J., 1990, "Remote sensing of the xanthophyll cycle and chlorophyll fluorescence in sunflower leaves and canopies," Oecologia, 85, pp. 1-7.

[62] Dekker, A., Brando, V., Anstee, J., Fyfe, S., Malthus, T., and Karpouzli, E., 2006, "Remote sensing of seagrass ecosystems: Use of spaceborne and airborne sensors," Larkum, A.W.D., Orth, R.J. and Duarte, C.M., eds, Seagrasses: Biology, Ecology and Conservation, Springer, Berlin, pp. 347-359.

[63] Curtiss, B. and Goetz, A. F. H., 1994, "Field spectrometry: Techniques and instrumentation," Proc. Int. Symp. Spectral Sensing Res., pp. 1-9.

[64] Masini, R. and Manning, C. R., 1997, "The photosynthetic responses to irradiance and temperature of four meadow-forming seagrasses," Aquat. Bot., 58, pp. 21-36.

[65] Larkum, A. W. D., Roberts, G., Kuo, J., and Strother, S., 1989, "Gaseous movement in seagrasses," Larkum, A.W.D., McComb, A.J., and Shepherd, S.A., eds, Biology of seagrasses: a treatise on the biology of seagrasses with special reference to the Australian region, Elsevier, New York, NY, pp. 686-722.

[66] Pérez-Llorens, J. L., Strother, S., and Niell, F. X., 1994, "Species differences in short-term pigment levels in four Australian seagrasses in response to dessication and rehydration," Botanica Marina, 37, pp. 91-95.

[67] Touchette, B. W. and Burkholder, J. M., 2000, "Overview of the physiological ecology of carbon metabolism in seagrasses," J. Exp. Mar. Biol. Ecol., 250, pp.

169-205.

[68] Lubin, D., Li, W., Dustan, P., Mazel, C., and Stamnes, K., 2001, "Spectral signatures of coral reefs: features from space," Remote Sens. Environ., 75, pp. 127-137.

[69] Diersson, H. M., Zimmerman, R. C., Leathers, R. A., Downes, T. V., and Davis, C. O., 2003, "Ocean colour remote sensing of seagrass and bathymetry in the Bahama Banks by high resolution airborne imagery," Limnology and Oceanography, 48, pp. 444-455.

[70] Kutser, T., Dekker, A. G., and Skirving, W., 2003, "Modeling spectral discrimination of Great Barrier Reef benthic communities by remote sensing instruments," Limnology and Oceanography, 48, pp. 497-510.

[71] Andréfouët, S., Payri, C., Hochberg, E., Che, L. M., and Atkinson, M. J., 2003, "Airborne hyperspectral detection of microbial mat pigmentation in Rangiroa atoll," Limnology and Oceanography, 48, pp. 426-430.